Nitro-fatty acid pharmacokinetics in the adipose tissue compartment[S]

Marco Fazzari,[*,†] **Nicholas K. H. Khoo,**[†] **Steven R. Woodcock,**[†] **Diane K. Jorkasky,**[§] **Lihua Li,**[†] **Francisco J. Schopfer,**[1,†] **and Bruce A. Freeman**[1,†]

Fondazione Ri.MED,* 90133 Palermo, Italy; Department of Pharmacology and Chemical Biology,[†] University of Pittsburgh, Pittsburgh, PA 15261; and Complexa Inc.,[§] Pittsburgh, PA 15203

Abstract Electrophilic nitro-FAs (NO_2-FAs) promote adaptive and anti-inflammatory cell signaling responses as a result of an electrophilic character that supports posttranslational protein modifications. A unique pharmacokinetic profile is expected for NO_2-FAs because of an ability to undergo reversible reactions including Michael addition with cysteine-containing proteins and esterification into complex lipids. Herein, we report via quantitative whole-body autoradiography analysis of rats gavaged with radiolabeled 10-nitro-[^{14}C] oleic acid, preferential accumulation in adipose tissue over 2 weeks. To better define the metabolism and incorporation of NO_2-FAs and their metabolites in adipose tissue lipids, adipocyte cultures were supplemented with 10-nitro-oleic acid (10-NO_2-OA), nitro-stearic acid, nitro-conjugated linoleic acid, and nitro-linolenic acid. Then, quantitative HPLC-MS/MS analysis was performed on adipocyte neutral and polar lipid fractions, both before and after acid hydrolysis of esterified FAs. NO_2-FAs preferentially incorporated in monoacyl- and diacylglycerides, while reduced metabolites were highly enriched in triacylglycerides. This differential distribution profile was confirmed in vivo in the adipose tissue of NO_2-OA-treated mice.[S] This pattern of NO_2-FA deposition lends new insight into the unique pharmacokinetics and pharmacologic actions that could be expected for this chemically-reactive class of endogenous signaling mediators and synthetic drug candidates.—Fazzari, M., N. K. H. Khoo, S. R. Woodcock, D. K. Jorkasky, L. Li, F. J. Schopfer, and B. A. Freeman. Nitro-fatty acid pharmacokinetics in the adipose tissue compartment. *J. Lipid Res.* 2017. 58: 375–385.

Supplementary key words adipocytes • lipolysis and fatty acid metabolism • metabolomics • mass spectrometry

Unsaturated FAs of cellular membranes, lipoproteins, and dietary fats are susceptible to oxidation and nitration by reactive oxygen species and nitrogen oxides during inflammatory and metabolic stress (1–3). In particular, the reaction between unsaturated FAs and the nitric oxide and nitrite (NO_2^-)-derived radical species nitrogen dioxide ($\cdot NO_2$) generates electrophilic FA nitro-alkene byproducts (NO_2-FAs) (4). These molecules are endogenously detected and have been observed to mediate salutary responses in models of inflammatory injury and oxidative stress. Current data supports that NO_2-FAs predominantly signal via posttranslational protein modifications, specifically of functionally significant Cys residues of nuclear transcription factor erythroid 2-related factor 2 (Nrf2), soluble epoxide hydrolase (sEH), p65 subunit of nuclear factor kappa B (NF-kB), transient receptor potential cation channel subfamily V member 1 (TRPV1), and heat shock factor-1 (HSF-1) (5–9).

NO_2-FAs have been detected in a variety of species, including mammals and plants, as both free acid and as complex lipid-esterified species (3, 10, 11). For example, NO_2-FAs are detected at micromolar concentrations in rodent cardiac mitochondria subjected to an episode of ischemia-reperfusion and at nanomolar concentrations in healthy human plasma and urine (12–14). Additionally, NO_2-FAs have been detected in Arabidopsis, fresh olives,

and extra virgin olive oil (15, 16). Notably, plasma and urinary NO$_2$-FA concentrations in humans are increased following oral supplementation with NO$_2^-$, nitrate (NO$_3^-$), and conjugated linoleic acid (CLA) (17, 18).

Recently, NO$_2$-FA-containing phospholipids have been identified in cardiac mitochondria isolated from an animal model of type 1 diabetes (10), and NO$_2$-FA-containing triacylglycerides (TAGs) have been detected in nitro-oleic acid (NO$_2$-OA)-supplemented adipocytes and plasma of rats after gavage with NO$_2$-OA (3). The analytical advances permitting the detection of FA nitro-alkene derivatives in complex lipids provide new opportunities for better understanding NO$_2$-FA pharmacokinetics, metabolism, and potential toxicology. To date, the identification and quantitation of NO$_2$-FAs in complex lipids has been limited by: *1*) the instability of NO$_2$-FAs during enzymatic and basic hydrolysis; *2*) the diversity of potential structures wherein NO$_2$-FAs can be incorporated (e.g., sterols, phospholipids, glycolipids, glycerolipids); *3*) challenges of the analysis NO$_2$-FA-containing complex lipids and their relative low abundance in cells and tissues; and *4*) the lack of synthetic standards (19, 20).

Herein, we show the preferential distribution of orally administered 10-nitro-[^{14}C]oleic acid radiolabeled at carbon 10 (10-NO$_2$-[^{14}C]OA) in adipose tissue of rats over a 2 week period via quantitative whole-body autoradiography (QWBA). Then, after lipid class fractionation, we report the quantitative analysis of the differential incorporation of NO$_2$-FA and metabolites into cultured adipocytes before and after acid hydrolysis, using HPLC-MS/MS. We observed the preferential incorporation of electrophilic versus nonelectrophilic NO$_2$-FAs in adipocyte mono- and di-acylglycerides (MAG+DAGs), a phenomenon confirmed in adipose tissue obtained from NO$_2$-OA-treated mice. These findings reveal tissue-specific pharmacokinetics and the preferential role of adipose tissue in distribution and metabolism of NO$_2$-FAs in vivo.

MATERIALS AND METHODS

Materials

Oleic acid (OA), CLA (catalog number UC-60A), and α-linolenic acid were from Nu-Check Prep, Inc. (Elysian, MN). The [^{13}C$_{18}$]labeled OA was obtained from Spectra Stable Isotopes (Columbia, MD). The [^{15}N]labeled sodium nitrate was purchased from Cambridge Isotope Laboratories (Tewksbury, MA). Deuterium-labeled 1-bromononane-6,6,7,7-d_4 was obtained from CDN Isotopes (Quebec, Canada). The 10-NO$_2$-[^{14}C]OA (labeled at carbon 10) was synthesized by ABC Laboratories, Inc. (Columbia, MO). Nitro-linolenic acid (NO$_2$-LnA), nonspecific 9- and 10-nitro-octadec-9-enoic acid (NO$_2$-OA), and isotopically labeled analog nitro-[^{13}C$_{18}$]octadec-9-enoic acid (NO$_2$-[^{13}C$_{18}$]OA) were synthesized by direct alkene nitroselenation of the corresponding native FAs, as previously described (21). Nitro-CLA (NO$_2$-CLA) was synthesized according to a previously described method for conjugated diene nitration (11). The [^{15}N]nitro-[D$_4$]octadecenoic acid (NO$_2$-[^{15}N/D$_4$]OA) was synthesized from the corresponding isotopically labeled precursor, 1-[^{15}N]nitrononane-6,6,7,7-d_4 (obtained

by nucleophilic substitution of [^{15}N]labeled sodium nitrate and 1-bromononane-6,6,7,7-d_4) and a nine-carbon aldehyde-ester via a previously described nitroaldol procedure (21, 22). Nitro-stearic acid (NO$_2$-SA) and its isotopically labeled analog, [^{15}N]nitro-[D$_4$] octadecanoic acid (NO$_2$-[^{15}N/D$_4$]SA), were synthesized by selective reduction with sodium borohydride of the nitro-alkene double bond in NO$_2$-OA and NO$_2$-[^{15}N/D$_4$]OA, respectively. Nitro-alkene standards of various lengths (C$_{16}$, C$_{15}$, C$_{14}$, C$_{13}$, and C$_{12}$) were synthesized by nitroselenation (21) of the corresponding native FAs and used as calibrators to normalize for MS responses. Before each experiment, NO$_2$-OA, NO$_2$-CLA, and NO$_2$-LnA concentrations were measured spectrophotometrically in methanol using the following extinction coefficients: ε_{312} = 11,200 M^{-1}cm^{-1} for NO$_2$-CLA, ε_{257} = 7,000 M^{-1}cm^{-1} for NO$_2$-OA , and ε_{305} = 7,000 M^{-1}cm^{-1} for NO$_2$-LnA (21). DMEM, FBS, HBSS, and antibiotic-antimycotic solutions were from Corning Cellgro (Herndon, VA). Strata NH$_2$ solid phase extraction columns (55 μm, 70 A) were from Phenomenex (Torrance, CA). Solvents were LC-MS grade from Burdick and Jackson (Muskegon, MI). Chemicals were of analytical grade and purchased from Sigma (St. Louis, MO) unless otherwise stated.

Cell culture

The 3T3-L1 preadipocytes were maintained and differentiated into adipocytes as previously (23). Fully differentiated adipocytes were then treated with 100 μM CLA or 5 μM OA, NO$_2$-SA, 10-nitro-oleic acid (10-NO$_2$-OA), NO$_2$-CLA, NO$_2$-LnA in HBSS. Aliquots of cellular media were obtained at 1, 2, 4, 8, and 24 h, spiked with 20 pmol NO$_2$-[^{13}C$_{18}$]OA and NO$_2$-[^{15}N/ D$_4$]SA as internal standards, extracted using the Bligh and Dyer method (24), dried under a stream of nitrogen and reconstituted in 0.2 ml methanol for HPLC-MS/MS analysis. At the end of the treatment, adipocytes were rinsed with cold PBS, scraped, and lipids extracted.

Quantitative whole-body autoradiography analysis

The 10-NO$_2$-[^{14}C]OA (labeled at carbon 10) was administered by a single oral gavage as a solution in sesame oil to male Sprague-Dawley rats (8–10 weeks old, n = 8) at a dose level of 30 mg/4 MBq/2 ml sesame oil per kilogram body weight. Rats were euthanized at 1, 6, 24, 48, 72, 120, 168, and 336 h after dose administration and QWBA was then carried out on the carcass of n = 1 animal for each time point. A frozen carcass was set in a block of 2% (w/v) aqueous carboxymethyl cellulose at −80°C. Samples of whole blood reference standards containing six different concentrations of radioactivity were placed into holes drilled into the block to facilitate signal calibration. The block was mounted onto the stage of a microtome in a cryostat maintained at −20°C. Sagittal sections (∼30 μm) were obtained at six different levels through the carcass of each animal: *1*) kidney; *2*) intra-orbital lacrimal gland; *3*) harderian gland; *4*) adrenal gland; *5*) half brain and thyroid; and *6*) brain and spinal cord. The sections, mounted on sectioning tape, were freeze-dried using a Lyolab B freeze-drier. One section from each level was exposed to imaging plates and an adjacent freeze-dried section at each level was mounted and used for reference purposes when evaluating the images. After exposure in a refrigerated lead-lined exposure box for 3 days, imaging plates were scanned using a FLA5000 radioluminography system. The electronic images were analyzed using an image analysis package (Seescan Densitometry software, version 2.0). The limits of quantification for the procedure corresponded to the lowest and highest calibration standards (0.12 to 528 μg equivalents of 10-NO$_2$-OA per gram). Wherever possible, the maximum area for each tissue within a single autoradiogram was defined for measurement. These radiolabeling experiments were conducted at Huntingdon Life Sciences (Cambridgeshire,

UK) with approval by the Huntingdon Life Sciences Ethical Review Process Committee.

Liquid scintillation analysis

Plasma and blood cell radioactivity was measured by liquid scintillation analysis using Wallac 1409 automatic liquid scintillation counters. Radioactivity in amounts less than twice that of the background concentration in the samples was considered to be below the limit of accurate quantification (BLQ).

Administration of NO$_2$-OA in high-fat diet mice

All murine studies were conducted with the approval of the University of Pittsburgh Institutional Animal Care and Use Committee (25). In brief, 6–8 week old male C57Bl/6j mice were subjected to high-fat diet (HFD) purchased from Research Diets Inc. (D12492; New Brunswick, NJ) for 20 weeks. Age-matched controls were maintained on a standard rodent chow diet (Pro Lab RHM 3000 rodent diet; PMI Feeds, Inc., St. Louis, MO). Mice were fed ad libitum for 20 weeks and given free access to water. At week 13.5 of the HFD study, mice were anesthetized with isoflurane before Alzet osmotic pumps (Cupertino, CA) containing vehicle (polyethylene glycol/ethanol, 92:8) or 9- and 10-NO$_2$-OA were implanted subcutaneously in the back region. The osmotic mini pump was set to deliver 8 mg NO$_2$-OA /kg/day. At the end of the 20th week, mice were euthanized and epididymal fat pads were quickly removed (n = 9 per treatment group), snap-frozen, and stored at −80°C. Sections of adipose tissues (∼100 mg) were homogenized in a bullet blender for 5 min in 0.8 ml phosphate buffer 50 mM pH 7.4, and lipids were extracted.

Adipocyte lipid analysis

Adipocyte and adipose tissue lipids were extracted according to Bligh and Dyer (24), dried under a stream of nitrogen, and dissolved in 0.5 ml hexane/methyl tert-butyl ether/acetic acid (100:3:0.3 v/v/v). Lipid classes were further resolved chromatographically using solid phase extraction Strata NH$_2$ columns loaded with 500 mg lipid per 6 ml bed volume (26, 27). Columns were preconditioned by washing twice with 2 ml acetone/water (7:1, v/v) and twice with 2 ml hexane. The samples solubilized in hexane/methyl tert-butyl ether/acetic acid were loaded on the columns and cholesterol esters (CEs), TAGs, MAG+DAGs, FFAs, phosphatidylcholines (PCs), phosphatidylethanolamines, phosphatidylserines, and phosphatidylinositols were sequentially eluted with 12 ml of hexane, hexane/chloroform/ethyl acetate (100:5:5, v/v/v), chloroform/2-propanol (2:1, v/v), diethyl ether/2% acetic acid, acetonitrile/1-propanol (2:1, v/v), methanol, isopropanol/methanolic HCl (4:1, v/v), and methanol/methanolic HCl (9:1, v/v), respectively. The solvents were evaporated under a stream of nitrogen and then CEs, TAGs, and MAG+DAGs were dissolved in 0.2 ml ethyl acetate, while FFAs and phospholipid fractions were solvated in 0.2 ml methanol. Direct injection MS analysis of each fraction confirmed lipid class abundance and composition.

Acid hydrolysis of lipid fractions

Fractionated lipid classes were hydrolyzed by a modification of a previously reported protocol (28). Fractions (10 μl) were spiked with 20 pmol NO$_2$-[^{13}C$_{18}$]OA/NO$_2$-[^{15}N/D$_4$]SA mix internal standards. To limit artifactual acid-catalyzed nitration reactions, 50 μl methanolic sulfanilamide (1 g/10 ml) was added to scavenge adventitious NO$_2^-$. Then, the mixture was dried and incubated with 500 μl acetonitrile/HCl (9:1, v/v) at 100°C for 1 h. To assess whether NO$_2$-FAs were present before hydrolysis, samples were also incubated with 500 μl acetonitrile/water (9:1, v/v). Then, 95 μl water or ammonium hydroxide was added to

samples before and after hydrolysis, respectively. Samples were vortexed, centrifuged at 18,000 g for 10 min at 4°C, and NO$_2$-FAs analyzed by HPLC-MS/MS. The full hydrolysis of TAG and phospholipid standards was assessed by TLC and iodine staining.

HPLC-MS

Analysis of NO$_2$-FAs was performed by HPLC-MS/MS using an analytical C18 Luna column (2 × 100 mm, 5 μm; Phenomenex) at a 0.6 ml/min flow rate, with a gradient solvent system consisting of water containing 0.1% acetic acid (solvent A) and acetonitrile containing 0.1% acetic acid (solvent B). Samples were chromatographically resolved using the following gradient program: 45–100% solvent B (0–8 min); 100% solvent B (8–10 min) followed by 2 min re-equilibration to initial conditions. NO$_2$-FAs were detected using an API4000 Q-trap triple quadrupole mass spectrometer (AB Sciex, San Jose, CA) equipped with an ESI source in negative mode. The following parameters were used: declustering potential, –75 V; collision energy, –35 eV; and a desolvation temperature of 650°C. NO$_2$-FAs and their corresponding metabolites were detected using the multiple reaction monitoring (MRM) transitions shown in supplemental Table S1. Quantification of NO$_2$-FAs in cell media over 24 h in adipocytes and adipose tissue was performed by stable isotopic dilution analysis using NO$_2$-OA and NO$_2$-SA calibration curves in the presence of NO$_2$-[^{13}C$_{18}$]OA (MRM 344.3/46) and NO$_2$-[^{15}N/D$_4$]SA (MRM 333.3/47) internal standards. Nitro-FAs of various lengths (C$_{16}$, C$_{15}$, C$_{14}$, C$_{13}$, and C$_{12}$ followed as MRMs 298.3/46, 284.3/46, 270.3/46, 256.3/46, and 242.3/46) were used as external calibrants to normalize the effect of nitro-FA chain length on MS response intensity. Coefficient responses were obtained by plotting ion counts versus carbon chain length at fixed concentrations (supplemental Fig. S1).

RESULTS

Tissue distribution of radiolabeled NO$_2$-OA

QWBA revealed the tissue distribution of NO$_2$-OA over time. After oral administration of a single dose of 10-NO$_2$-[^{14}C]OA (30 mg/kg) to rats, radioactivity was readily absorbed from the gastrointestinal tract and widely distributed throughout the animal body. The vast majority of tissues reached maximum radiolabel distribution by 6 h after dosing (**Table 1**, supplemental Table S2), with radioactivity concentrations declining in most tissues by 24 h. Notably, brown and abdominal white adipose tissue displayed the highest levels of radioactivity 72 h postdosing in comparison with other organs, affirming that NO$_2$-FA and potential metabolites preferentially accumulate in adipose tissue (**Fig. 1**).

NO$_2$-FA distribution and metabolism in cultured adipocytes

To better characterize the distribution of NO$_2$-FA and metabolites in cellular lipid fractions, cultured 3T3-L1 adipocytes were supplemented with the biologically relevant mono- and poly-unsaturated nitro-alkenes, 10-NO$_2$-OA, NO$_2$-CLA, and NO$_2$-LnA, and the saturated nitro-alkane, NO$_2$-SA. The quantitation of NO$_2$-FAs before and after acid hydrolysis of adipocyte lipids revealed specific patterns of incorporation, intracellular distribution, and metabolism in each lipid fraction. As expected, free acid nitrated species

TABLE 1. Time-dependent distribution of radioactivity in rat tissues after oral administration of 10-NO$_2$-[^{14}C]OA

Tissue/Organ	Microgram Equivalents 10-NO$_2$-OA per Gram							
	1 h	6 h	24 h	48 h	72 h	120 h	168 h	336 h
Plasma[a]	11.2	**19.6**	1.48	0.625	0.338	0.207	0.122	BLQ
Brain	0.358	**1.72**	0.215	0.373	0.270	0.202	0.163	BLQ
Kidney medulla	17.3	**28.8**	2.08	0.931	0.682	0.441	0.324	1.12
Liver	16.7	**28.5**	4.48	1.97	1.19	0.741	0.509	0.299
Lungs	4.16	**17.2**	1.52	1.62	0.783	0.450	0.351	0.275
Heart (myocardium)	11.3	**19.0**	1.77	1.71	1.19	1.20	0.710	2.21
Fat (abdominal)[b]	1.77	**11.1**	4.57	3.10	5.60	7.81	3.87	5.49
Fat (brown)	8.52	43.1	41.3	**84.0**	11.9	10.6	3.75	3.03
Muscle (skeletal)	0.931	**1.64**	0.356	0.291	0.307	0.211	0.233	0.202
Stomach wall (non-glandular)	38.3	**555**[c]	19.6	7.04	1.35	0.827	0.361	0.189

Radioactivity levels in selected rat tissues were determined by QWBA following a single oral administration of 30 mg/kg 10-NO$_2$-[^{14}C]OA (labeled at carbon 10) (n = 1 for each time point). Values in bold represent maximum tissue concentrations (C$_{max}$).

[a]Determined by direct liquid scintillation analysis.

[b]Tissue corrected for quenching.

[c]Value should be treated as an estimate as above the upper limit of quantification.

were only detectable in the FFA fraction before hydrolysis. Neither elongation products nor metabolites shorter than C$_{12}$ were observed for all NO$_2$-FA treatments.

NO$_2$-OA was principally reduced to NO$_2$-SA and metabolized to its corresponding dinor, tetranor and hexanor β-oxidation products (3, 29). Esterified NO$_2$-OA was ~18 times more abundant in MAG+DAG than in TAG (**Fig. 2A**), while the nonelectrophilic NO$_2$-SA and its β-oxidation metabolites showed the opposite distribution. The NO$_2$-SA metabolite and its dinor, tetranor, and hexanor β-oxidation
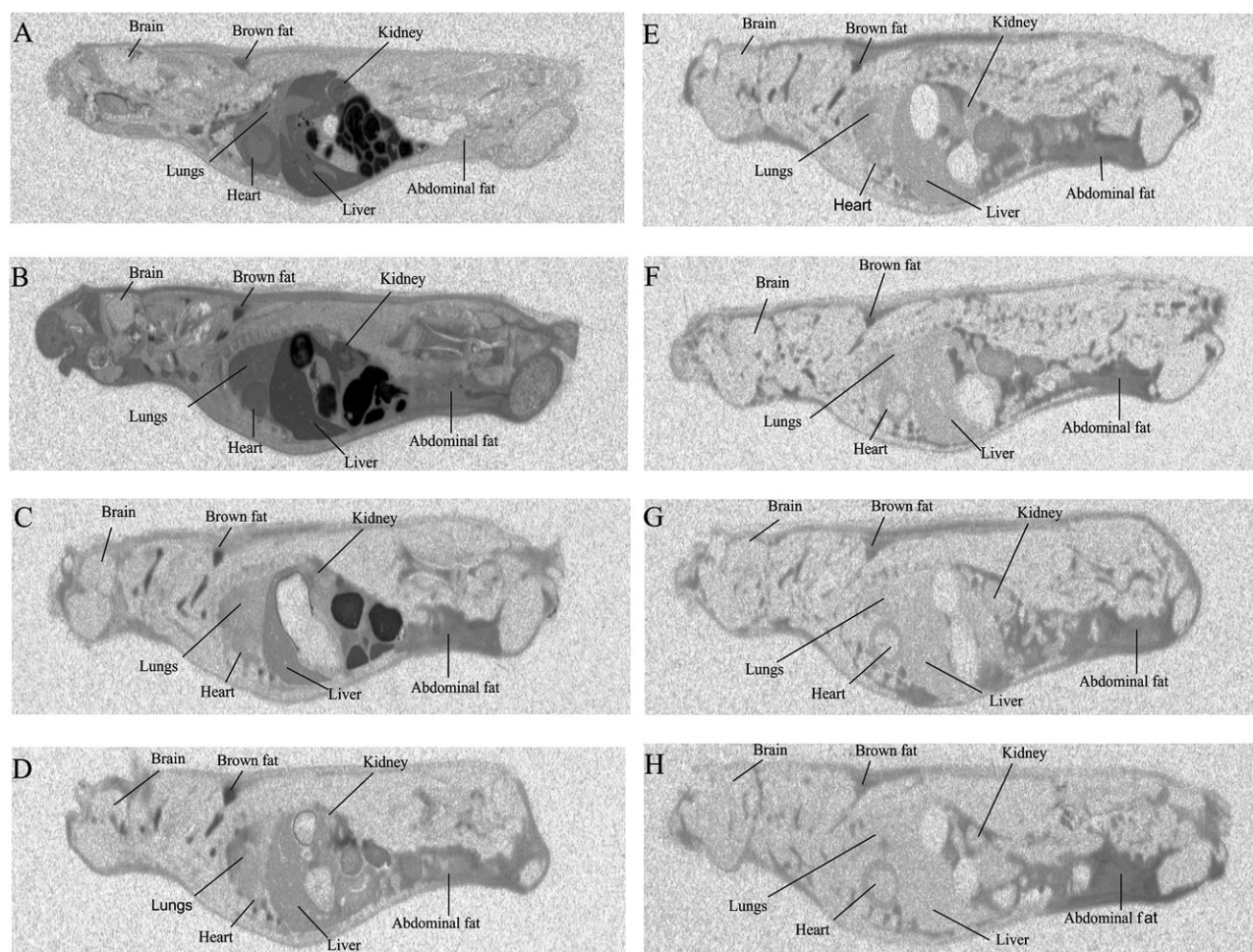
Fig. 1. Distribution of radioactivity in rats after a single oral administration of radiolabeled 10-NO$_2$-OA. Whole-body autoradiograms of rats euthanized at 1 h (A), 6 h (B), 24 h (C), 48 h (D), 72 h (E), 120 h (F), 168 h (G), and 336 h (H) after an oral administration of 30 mg/kg 10-NO$_2$-[^{14}C]OA (labeled at carbon 10). Radioactivity appears in black (n = 1 for each time point).
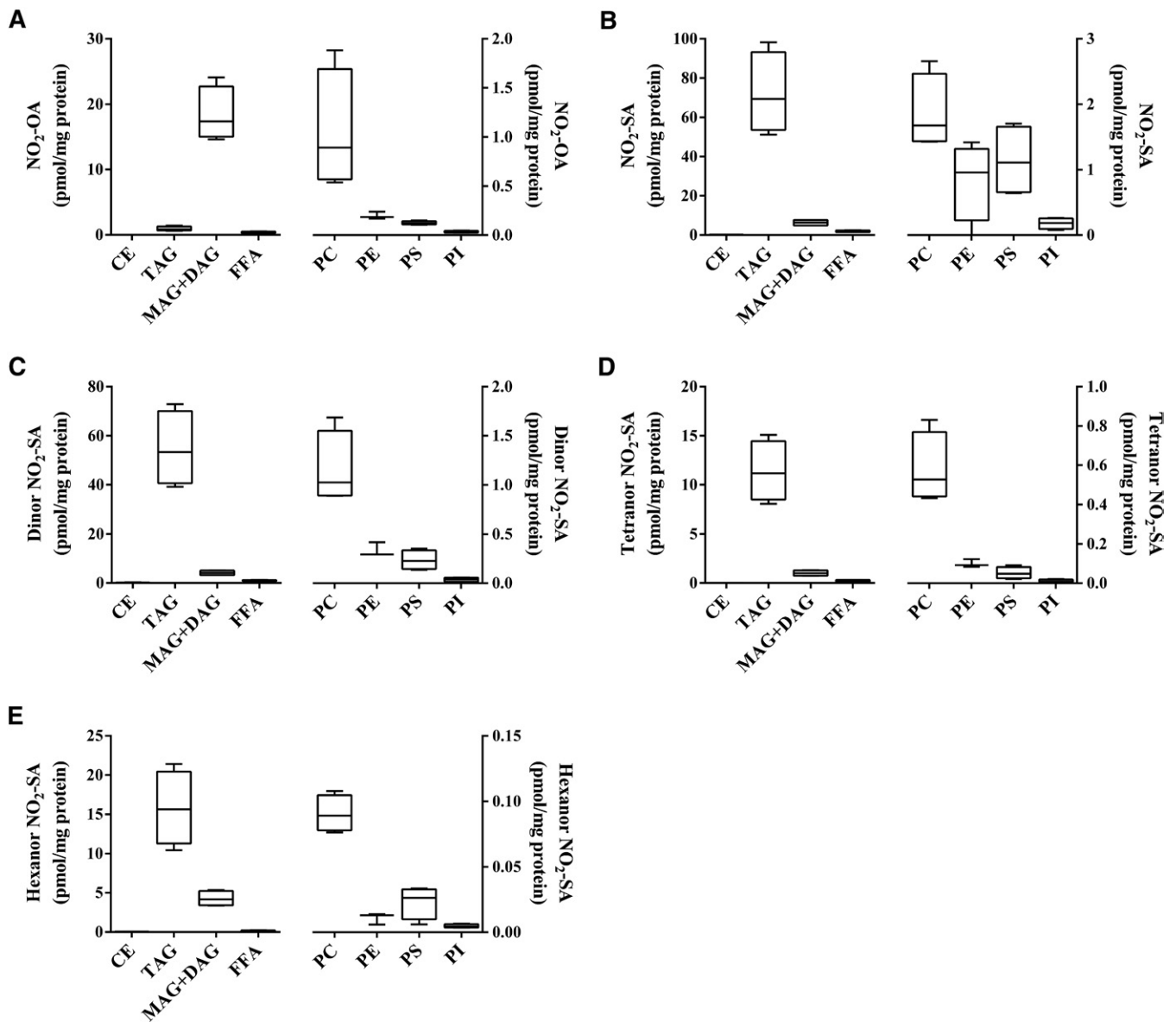
Fig. 2. Metabolism and distribution of NO$_2$-OA in lipid fractions of NO$_2$-OA-supplemented adipocytes. Fractionated lipid classes from adipocytes were analyzed by HPLC-MS/MS in negative ion mode after acid hydrolysis to determine the cellular content (picomoles per milligram protein) of NO$_2$-OA (A), NO$_2$-SA (B), dinor NO$_2$-SA (C), tetranor NO$_2$-SA (D), and hexanor NO$_2$-SA (E). FFA fraction was not hydrolyzed. Two independent experiments were performed. Range (minimum-maximum) and mean of one representative experiment (n = 4) are shown.

products were ~11-fold (Fig. 2B), ~13-fold (Fig. 2C), ~11-fold (Fig. 2D), and ~3.7-fold (Fig. 2E) more abundant in TAG than in MAG+DAG, respectively. This preferential incorporation of nitro-alkane metabolites was also confirmed in NO$_2$-SA-supplemented adipocytes, with NO$_2$-SA, dinor, tetranor, and hexanor β-oxidation products showing a lower relative distribution ratio (~2- to 3-fold) than the corresponding nitro-alkane metabolites stemming from the metabolism of NO$_2$-OA (**Fig. 3A–D**).

The dienoic nitro-alkene, NO$_2$-CLA, showed a profile of complex lipid partitioning that was similar to NO$_2$-OA, with the proviso that net extents of neutral lipid esterification were 10- to 20-fold lower (**Fig. 4A**). As for the distribution of NO$_2$-SA metabolites, the reduced metabolite of NO$_2$-CLA (NO$_2$-dihydro-CLA) and its dinor and tetranor β-oxidation

products were more abundant in TAG than in MAG+DAG fractions (Fig. 4B–D). Consistent with this trend, adipocytes supplemented with the trienoic nitro-alkene, NO$_2$-LnA, exhibited even lower levels of esterification compared with mono- and di-unsaturated nitro-alkenes. The NO$_2$-LnA levels in TAG and MAG+DAG fractions were similar (**Fig. 5A**). NO$_2$-dihydro-LnA, the nonelectrophilic reduced metabolite of NO$_2$-LnA, and its β-oxidation product dinor, NO$_2$-dihydro-LnA, had levels and lipid distributions that were similar to those of NO$_2$-SA and reduced NO$_2$-CLA metabolites (Fig. 5B, C). Notably, lower extents of NO$_2$-FA incorporation occurred in glycerophospholipid fractions as opposed to glycerolipid fractions (Figs. 2–5), with PC showing the highest levels among phospholipids likely due to its greater abundance (30, 31).
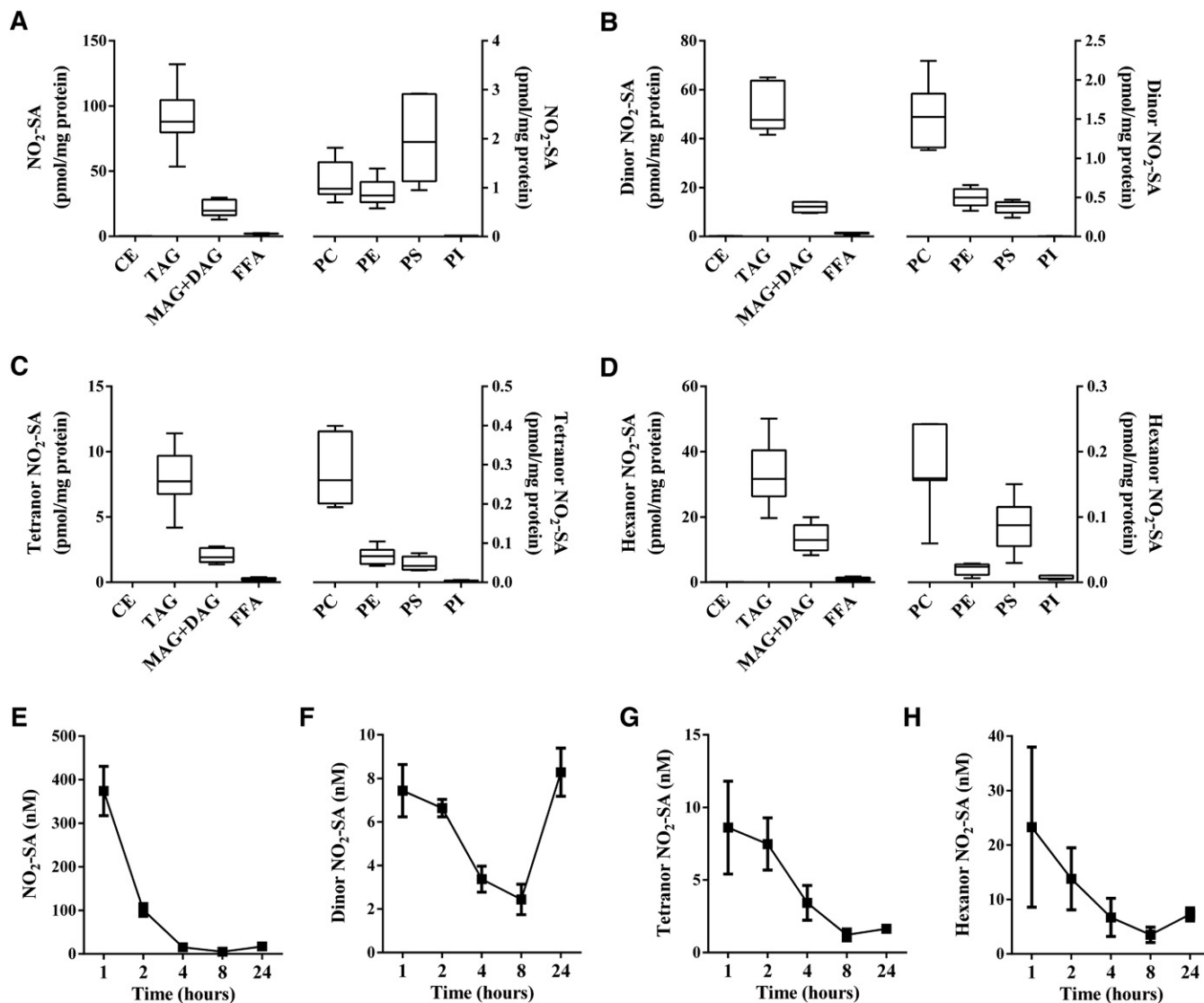
Fig. 3. Distribution and metabolic profile of NO$_2$-SA in NO$_2$-SA-supplemented adipocyte lipids and media. Adipocyte content (picomoles per milligram protein) of NO$_2$-SA (A), dinor NO$_2$-SA (B), tetranor NO$_2$-SA (C), and hexanor NO$_2$-SA (D) at 24 h after acid hydrolysis of fractionated lipid classes. FFA fraction was analyzed without hydrolysis. Time-dependent concentration changes in media of NO$_2$-SA and its metabolites (E), dinor NO$_2$-SA (F), tetranor NO$_2$-SA (G), and hexanor NO$_2$-SA (H). Range (minimum-maximum) and mean (A–D) and mean ± SD (E–H) are shown. Two independent experiments were performed (n ≥ 3).

## Distribution of metabolites of NO$_2$-FA in adipocyte culture media

NO$_2$-SA, NO$_2$-CLA, and NO$_2$-LnA metabolites were detected in the media of cultured adipocytes. The non-electrophilic nitro-alkane, NO$_2$-SA, was shown to rapidly convert into the shorter chain length NO$_2$-containing β-oxidation products, dinor, tetranor, and hexanor NO$_2$-SA, and was transported out of the cell (Fig. 3E–H). The electrophilic NO$_2$-CLA was reduced to primarily nonelectrophilic NO$_2$-dihydro-CLA (Fig. 4E), which underwent β-oxidation to yield dinor NO$_2$-dihydro-CLA and dinor NO$_2$-CLA, respectively (Fig. 4F). Further 12 and 14 carbon β-oxidation products were not detected. All NO$_2$-SA and NO$_2$-CLA nitro-alkane metabolites modestly increased in concentration between 8 and 24 h. NO$_2$-LnA metabolites were not detected as rapidly as NO$_2$-SA and NO$_2$-CLA metabolic products in the media and yielded

mainly the reduced metabolite, NO$_2$-dihydro-LnA (Fig. 5D), and dinor and tetranor β-oxidation products (Fig. 5E, F).

NO$_2$-OA esterification and metabolism in adipose tissue in vivo

The QWBA study coupled with the distribution and metabolism of nitro-alkenes and nitro-alkanes in cultured adipocytes encouraged testing whether NO$_2$-FAs could be detected in adipose tissue in vivo in a clinically-relevant model system. A HFD-induced murine model of obesity demonstrates inflammatory responses akin to humans, in part characterized by the increased generation of reactive nitric oxide and oxygen-derived reactive species, which could potentially give rise to esterified NO$_2$-FAs (32–34). However, analysis of lipid fractions from adipose tissue of HFD-control mice did not show the presence
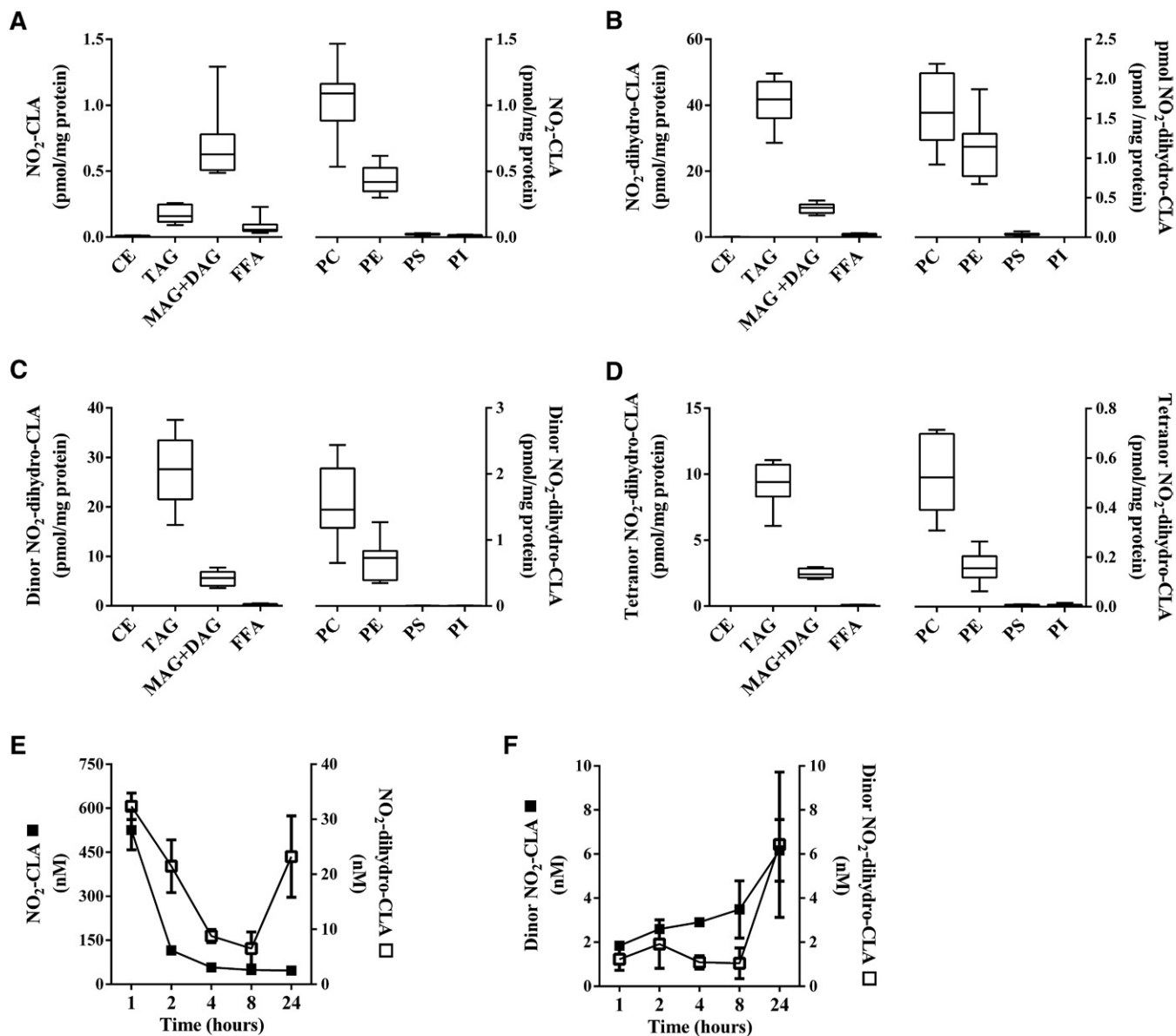
Fig. 4. Distribution and metabolic profile of NO_2-CLA in NO_2-CLA-supplemented adipocyte lipids and media. Cellular content of NO_2-CLA (A), NO_2-dihydro-CLA (B), dinor NO_2-dihydro-CLA (C), and tetranor NO_2-dihydro-CLA (D) at 24 h was established on fractionated lipid classes after acid hydrolysis. FFA fraction was not subjected to acid hydrolysis. Concentration of nitro-FA species was determined in media for the following species: NO_2-CLA (filled square) and NO_2-dihydro-CLA (open square) (E) and dinor NO_2-CLA (filled square) and dinor NO_2-dihydro-CLA (open square) (F) over a period of 24 h. Range (minimum-maximum) and mean (A–D) and mean ± SD (E, F) are shown. Two independent experiments were performed (n = 4).

of NO_2-FAs (data not shown). Recent reports indicate that NO_2-OA promotes beneficial metabolic and anti-inflammatory responses by modulating Nrf2-dependent antioxidant gene expression, sEH activity, and TLR4/NF-kB signaling (6–8). The administration of pure synthetic NO_2-OA induces beneficial signaling actions and physiological responses in animal models of metabolic, vascular, renal, and pulmonary disease (12). The safety of NO_2-OA use as a drug candidate in humans has been tested by multiple phase I studies. With Food and Drug Administration approval, NO_2-OA is now undergoing phase II clinical trials. For these reasons, we considered it important to better understand FA nitro-alkene pharmacokinetics,

specifically the incorporation of NO_2-OA and its metabolites into adipose tissue complex lipids after NO_2-OA supplementation. Notably, as for in vitro study observations, NO_2-OA was esterified to neutral glycerolipids and more abundant in the MAG+DAG than in the TAG fraction (**Fig. 6A**), while its nitro-alkane metabolites, such as NO_2-SA and dinor, tetranor, and hexanor NO_2-SA, were preferentially distributed in TAG fractions (Fig. 6B–E). No NO_2-FAs were detected in the phospholipid fraction, either before or after hydrolysis. Very low levels of NO_2-OA were present in the FFA fraction (Fig. 6A), along with reduced and β-oxidation products. Similarly, low amounts of NO_2-OA were detected in CE fractions.
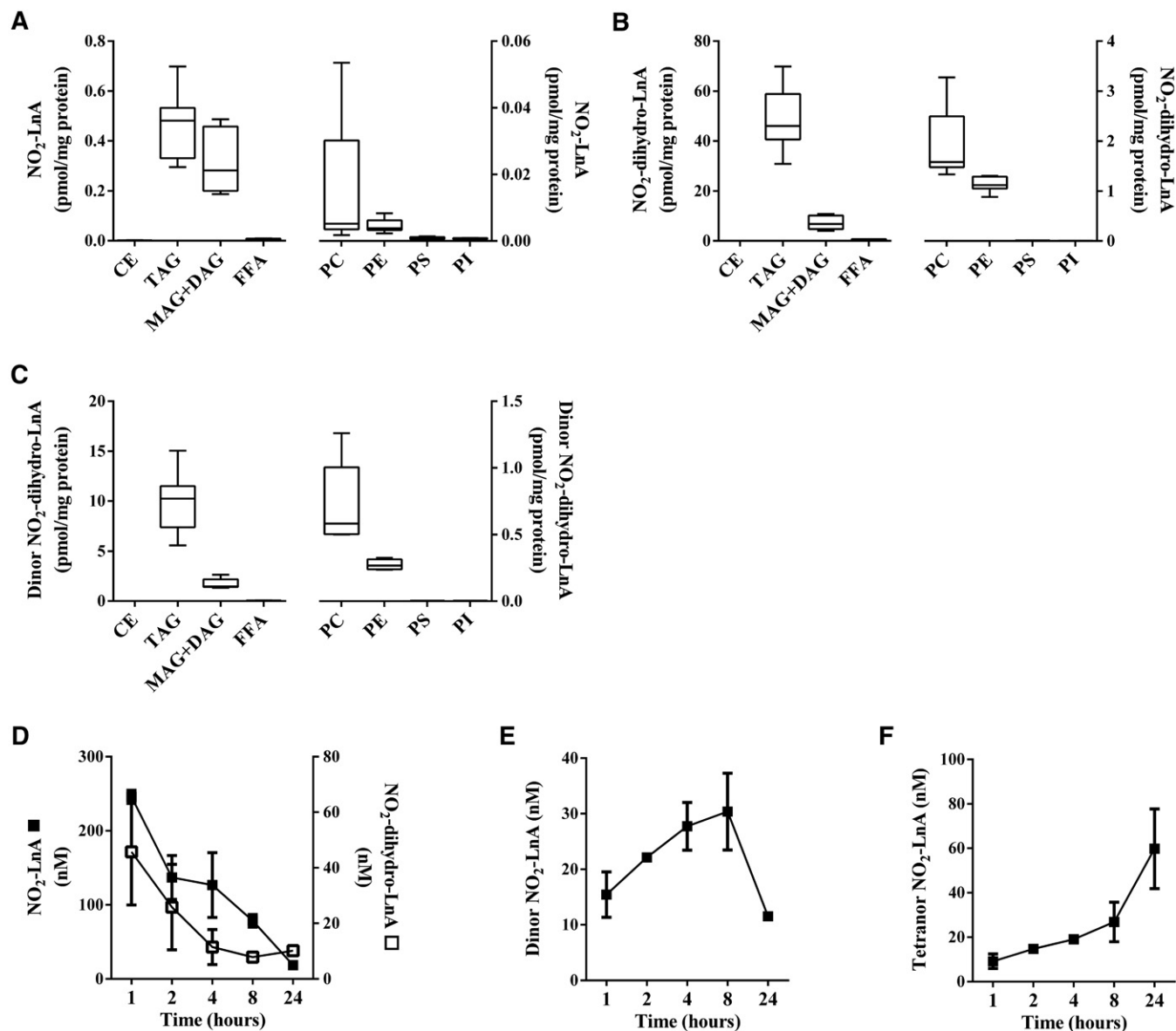
Fig. 5. Distribution and metabolic profile of NO_2-LnA in NO_2-LnA-supplemented adipocyte lipids and media. Adipocyte cellular content of NO_2-LnA (A), NO_2-dihydro-LnA (B), and dinor NO_2-dihydro-LnA (C) at 24 h, after acid hydrolysis of the different fractionated lipid classes. FFA fraction was analyzed without hydrolysis. Time-dependent concentration changes of NO_2-LnA (filled square) and its metabolites NO_2-dihydro-LnA (open square) (D), dinor NO_2-LnA (E), and tetranor NO_2-LnA (F). Range (minimum-maximum) and mean (A–C) and mean ± SD (D–F) are shown. Two independent experiments were performed (n ⩾ 3).

DISCUSSION

Nitration of unsaturated FAs and the corresponding generation of electrophilic NO_2-FA occur during acidic conditions of digestion and oxidative inflammatory conditions (3, 4, 17, 18, 35). The electrophilic properties of NO_2-FA induce anti-inflammatory and cytoprotective actions via reversible posttranslational modification of transcriptional regulatory proteins, such as NF-kB, Keap1/Nrf2, and PPAR-γ, and enzymes such as xanthine oxidoreductase and sEH (6–8, 36–38). Beneficial metabolic and anti-inflammatory effects of NO_2-FAs have been shown in animal models of fibrosis, atherosclerosis, renal and cardiac ischemia reperfusion, restenosis, and diabetes (12, 39–44).

NO_2-FAs are metabolized by various reactions, such as mitochondrial β-oxidation, Michael addition, enzyme-catalyzed reduction, and esterification into complex lipids (3, 14, 45, 46). Both nitro-alkenes and nitro-alkanes are metabolized by mitochondrial β-oxidation generating $(C_2H_4)_n$-shorter metabolites (14, 29, 47). In humans and rodents, metabolites as short as C_8 have been observed in urine (48). However, no nitro-C_{12}-alkenes and nitro-C_{10}-alkanes were detected in adipocytes, indicating that adipocytes lack the necessary mitochondrial or peroxisomal enzymatic machinery to further process nitro-alkenes through β-oxidation cycles when the nitro group is proximal to the carboxyl moiety (3, 14, 29). The electrophilic nature of nitro-alkenes undergoes: *1*) reversible Michael
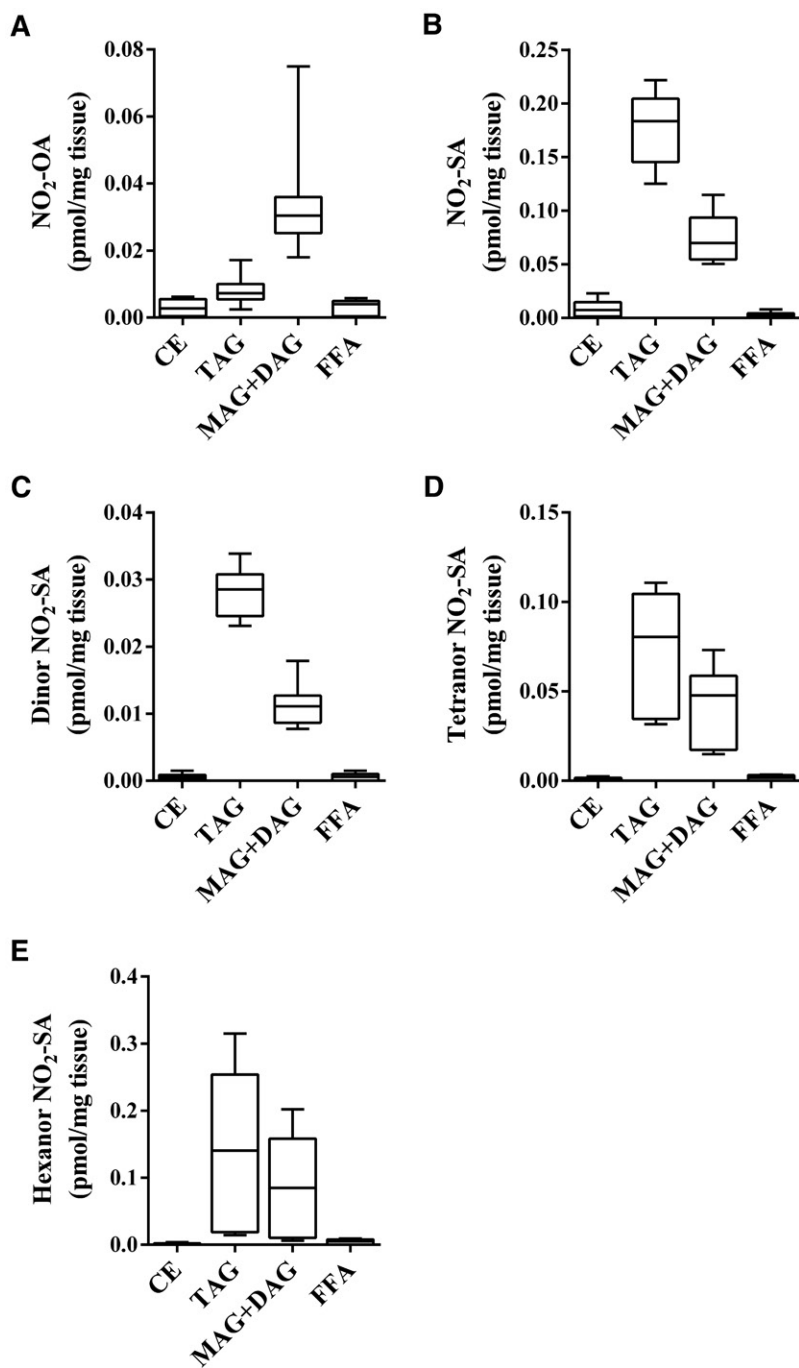
Fig. 6. Bio-distribution of NO$_2$-OA and its metabolites in adipose tissue of NO$_2$-OA-supplemented HFD-fed mice. NO$_2$-OA was delivered subcutaneously to mice on a HFD (8 mg/kg/day) for 6.5 weeks. Levels of NO$_2$-FAs on adipose tissue associated to the different lipid classes were evaluated after acid hydrolysis. The following species were followed: NO$_2$-OA (A); NO$_2$-SA (B); dinor NO$_2$-SA (C); tetranor NO$_2$-SA (D); and hexanor NO$_2$-SA (E). FFA fraction was not subjected to acid hydrolysis. Range (minimum-maximum) and mean of one experiment with n = 9 are shown.

addition with GSH and cysteine-containing proteins (4, 49, 50); and *2*) rapid metabolism by prostaglandin reductase-1 and resultant generation of inactive nitro-alkanes (47). These two metabolic reactions have a significant impact on the extra- and intra-cellular distribution of NO$_2$-FAs and downstream pharmacological effects. The time-dependent enrichment of nitro-alkene metabolites in the extracellular compartment could be a consequence of NO$_2$-FA-GSH adduct export via multidrug resistance protein-1. This, in the presence of low extracellular GSH concentrations, can more readily dissociate to regenerate free nitro-alkenes or be passively transported across the cellular membrane, a pathway also shared by nitro-alkane metabolites (49–51). Furthermore, the extracellular time-dependent decrease

in nitro-alkane metabolites could reflect their cellular reuptake and esterification into complex lipids. In this regard, the incorporation of NO$_2$-FAs into CoA, phospholipid, and TAG has been reported (3, 10), but little is known about the amount and the differential esterification of NO$_2$-FA and metabolites into complex cellular lipids.

Notably, 10-NO$_2$-OA is now entering Food and Drug Administration-approved phase II clinical trials, motivating an even better understanding of pathways that might impact NO$_2$-FA pharmacokinetics. Herein, the QWBA analysis of 10-NO$_2$-[^{14}C]OA (labeled at carbon 10) in rats revealed absorption into the systemic circulation and distribution throughout all tissue compartments, reaching the highest concentrations within 6 h after oral dosing and then

declining over the course of 2 weeks. Radiolabel distribution was prominent in brown and abdominal adipose tissue, in part due to the lipophilic nature of 10-NO$_2$-OA. One limitation of the QWBA study is that the radioactivity measured in tissues by autoradiography could be either native 10-NO$_2$-OA or metabolites that retain carbon 10. In order to better define the pharmacology of the parent molecule, its still-electrophilic β-oxidation products, and non-electrophilic (reduced) metabolites, quantitative analysis of these species was performed in NO$_2$-FA-rich adipose tissue by HPLC-MS/MS.

Pharmacokinetics studies of electrophilic FAs have principally focused on the FFA species. Recently, qualitative studies of the esterification of FA electrophiles into phospholipids and TAGs have been reported (3, 10, 14, 29, 47). The quantitative analysis of NO$_2$-FA containing complex lipids or free NO$_2$-FAs after de-esterification reactions is methodologically challenging and lacks synthetic standards. Also, the quantitation of free NO$_2$-FAs after enzymatic and basic hydrolysis of cellular lipids can artifactually impact quantitative analysis, due by the instability of acyl nitro-alkenes in neutral and basic aqueous solutions (19, 20). Thus, an acid hydrolysis method was devised that assured the stability of esterified and hydrolyzed NO$_2$-FAs. The advantages of this method over enzymatic hydrolysis of TAGs and phospholipids include a faster and more efficient hydrolysis. Enzymatic reactions are overall slower, generate partial hydrolysis products (diacylglycerides, monoacylglycerides, and lysophospholipids), and can result in lipid electrophile reactions with the protein and thiol reductants present in lipases. Thus, acid hydrolysis provided a faster and more complete de-esterification of complex lipids and allowed for the quantification of de-esterified NO$_2$-FAs in adipocytes and adipose tissue before and after acid hydrolysis (28). This in turn shed light on electrophilic and nonelectrophilic NO$_2$-FA metabolism, distribution, and incorporation into cellular lipids.

In the intracellular compartment of adipocytes, both nitro-alkenes and nitro-alkanes showed preferential incorporation into MAG+DAG and TAG lipids, respectively, which could be a result of differential NO$_2$-FA intracellular availability (free vs. protein-adducted lipid), trafficking, and metabolism (52). For example, NO$_2$-FAs readily form CoA thioesters that are then distributed into different catabolic or anabolic reactions, making them a hub for metabolic processes (29). As long-chain acyl-CoA synthetase isoforms have FA preferences and tissue expression (53), nitro-alkenes and nitro-alkanes could differentially generate electrophilic NO$_2$-FA-CoA esters, which in turn may modulate the activity of enzymes responsible for their incorporation into glycerolipids and phospholipids.

In summary, the esterification of fatty acyl nitro-alkene derivatives into MAG+DAG and PC reveals a unique pharmacokinetic character of NO$_2$-FAs, wherein adipose tissue MAG+DAG and to a lesser extent TAG represent an intermediate reservoir of still-electrophilic nitro-alkene species that can impact the signaling actions of this class of mediators.■

REFERENCES

1. Guillén, M. D., and E. Goicoechea. 2008. Toxic oxygenated alpha,beta-unsaturated aldehydes and their study in foods: a review. *Crit. Rev. Food Sci. Nutr.* **48:** 119–136.

2. O'Donnell, V. B., J. P. Eiserich, P. H. Chumley, M. J. Jablonsky, N. R. Krishna, M. Kirk, S. Barnes, V. M. Darley-Usmar, and B. A. Freeman. 1999. Nitration of unsaturated fatty acids by nitric oxide-derived reactive nitrogen species peroxynitrite, nitrous acid, nitrogen dioxide, and nitronium ion. *Chem. Res. Toxicol.* **12:** 83–92.

3. Fazzari, M., N. Khoo, S. R. Woodcock, L. Li, B. A. Freeman, and F. J. Schopfer. 2015. Generation and esterification of electrophilic fatty acid nitroalkenes in triacylglycerides. *Free Radic. Biol. Med.* **87:** 113–124.

4. Freeman, B. A., P. R. Baker, F. J. Schopfer, S. R. Woodcock, A. Napolitano, and M. d'Ischia. 2008. Nitro-fatty acid formation and signaling. *J. Biol. Chem.* **283:** 15515–15519.

5. Villacorta, L., J. Zhang, M. T. Garcia-Barrio, X. L. Chen, B. A. Freeman, Y. E. Chen, and T. Cui. 2007. Nitro-linoleic acid inhibits vascular smooth muscle cell proliferation via the Keap1/Nrf2 signaling pathway. *Am. J. Physiol. Heart Circ. Physiol.* **293:** H770–H776.

6. Charles, R. L., O. Rudyk, O. Prysyazhna, A. Kamynina, J. Yang, C. Morisseau, B. D. Hammock, B. A. Freeman, and P. Eaton. 2014. Protection from hypertension in mice by the Mediterranean diet is mediated by nitro fatty acid inhibition of soluble epoxide hydrolase. *Proc. Natl. Acad. Sci. USA.* **111:** 8167–8172.

7. Villacorta, L., L. Chang, S. R. Salvatore, T. Ichikawa, J. Zhang, D. Petrovic-Djergovic, L. Jia, H. Carlsen, F. J. Schopfer, B. A. Freeman, et al. 2013. Electrophilic nitro-fatty acids inhibit vascular inflammation by disrupting LPS-dependent TLR4 signalling in lipid rafts. *Cardiovasc. Res.* **98:** 116–124.

8. Kansanen, E., G. Bonacci, F. J. Schopfer, S. M. Kuosmanen, K. I. Tong, H. Leinonen, S. R. Woodcock, M. Yamamoto, C. Carlberg, S. Yla-Herttuala, et al. 2011. Electrophilic nitro-fatty acids activate NRF2 by a KEAP1 cysteine 151-independent mechanism. *J. Biol. Chem.* **286:** 14019–14027.

9. Zhang, X., K. B. Koronowski, L. Li, B. A. Freeman, S. Woodcock, and W. C. de Groat. 2014. Nitro-oleic acid desensitizes TRPA1 and TRPV1 agonist responses in adult rat DRG neurons. *Exp. Neurol.* **251:** 12–21.

10. Melo, T., P. Domingues, R. Ferreira, I. Milic, M. Fedorova, S. M. Santos, M. A. Segundo, and M. R. Domingues. 2016. Recent advances on mass spectrometry analysis of nitrated phospholipids. *Anal. Chem.* **88:** 2622–2629.

11. Woodcock, S. R., S. R. Salvatore, G. Bonacci, F. J. Schopfer, and B. A. Freeman. 2014. Biomimetic nitration of conjugated linoleic acid: formation and characterization of naturally occurring conjugated nitrodienes. *J. Org. Chem.* **79:** 25–33.

12. Rudolph, V., T. K. Rudolph, F. J. Schopfer, G. Bonacci, S. R. Woodcock, M. P. Cole, P. R. Baker, R. Ramani, and B. A. Freeman. 2010. Endogenous generation and protective effects of nitro-fatty acids in a murine model of focal cardiac ischaemia and reperfusion. *Cardiovasc. Res.* **85:** 155–166.

13. Lima, E. S., P. Di Mascio, H. Rubbo, and D. S. Abdalla. 2002. Characterization of linoleic acid nitration in human blood plasma by mass spectrometry. *Biochemistry.* **41:** 10717–10722.

14. Salvatore, S. R., D. A. Vitturi, P. R. S. Baker, G. Bonacci, J. R. Koenitzer, S. R. Woodcock, B. A. Freeman, and F. J. Schopfer. 2013. Characterization and quantification of endogenous fatty acid nitroalkene metabolites in human urine. *J. Lipid Res.* **54:** 1998–2009.

15. Mata-Pérez, C., B. Sánchez-Calvo, M. N. Padilla, J. C. Begara-Morales, F. Luque, M. Melguizo, J. Jiménez-Ruiz, A. Fierro-Risco, A. Peñas-Sanjuán, R. Valderrama, et al. 2016. Nitro-fatty acids in plant signaling: nitro-linolenic acid induces the molecular chaperone network in Arabidopsis. *Plant Physiol.* **170:** 686–701.

16. Fazzari, M., A. Trostchansky, F. J. Schopfer, S. R. Salvatore, B. Sanchez-Calvo, D. Vitturi, R. Valderrama, J. B. Barroso, R. Radi, B. A. Freeman, et al. 2014. Olives and olive oil are sources of electrophilic fatty acid nitroalkenes. *PLoS One.* **9:** e84884.

17. Delmastro-Greenwood, M., K. S. Hughan, D. A. Vitturi, S. R. Salvatore, G. Grimes, G. Potti, S. Shiva, F. J. Schopfer, M. T. Gladwin, B. A. Freeman, et al. 2015. Nitrite and nitrate-dependent generation of anti-inflammatory fatty acid nitroalkenes. *Free Radic. Biol. Med.* **89:** 333–341.

18. Bonacci, G., F. Schopfer, S. Salvatore, T. K. Rudolph, V. Rudolph, K. Khoo, J. Koenitzer, F. Golin-Bisello, P. R. Baker, D. Shores, et al. 2012. Conjugated linoleic acid a preferential substrate for fatty acid nitration. *J. Biol. Chem.* **287:** 44071–44082.

19. Manini, P., L. Capelli, S. Reale, M. Arzillo, O. Crescenzi, A. Napolitano, V. Barone, and M. d'Ischia. 2008. Chemistry of nitrated lipids: remarkable instability of 9-nitrolinoleic acid in neutral aqueous medium and a novel nitronitrate ester product by concurrent autoxidation/nitric oxide-release pathways. *J. Org. Chem.* **73:** 7517–7525.

20. Schopfer, F. J., P. R. Baker, G. Giles, P. Chumley, C. Batthyany, J. Crawford, R. P. Patel, N. Hogg, B. P. Branchaud, J. R. Lancaster, Jr., et al. 2005. Fatty acid transduction of nitric oxide signaling. Nitrolinoleic acid is a hydrophobically stabilized nitric oxide donor. *J. Biol. Chem.* **280:** 19289–19297.

21. Woodcock, S. R., G. Bonacci, S. L. Gelhaus, and F. J. Schopfer. 2013. Nitrated fatty acids: synthesis and measurement. *Free Radic. Biol. Med.* **59:** 14–26.

22. Woodcock, S. R., A. J. Marwitz, P. Bruno, and B. P. Branchaud. 2006. Synthesis of nitrolipids. All four possible diastereomers of nitrooleic acids: (E)- and (Z)-, 9- and 10-nitro-octadec-9-enoic acids. *Org. Lett.* **8:** 3931–3934.

23. Khoo, N. K., L. Mo, S. Zharikov, C. Kamga-Pride, K. Quesnelle, F. Golin-Bisello, L. Li, Y. Wang, and S. Shiva. 2014. Nitrite augments glucose uptake in adipocytes through the protein kinase A-dependent stimulation of mitochondrial fusion. *Free Radic. Biol. Med.* **70:** 45–53.

24. Bligh, E. G., and W. J. Dyer. 1959. A rapid method of total lipid extraction and purification. *Can. J. Biochem. Physiol.* **37:** 911–917.

25. Kelley, E. E., J. Baust, G. Bonacci, F. Golin-Bisello, J. E. Devlin, C. M. St Croix, S. C. Watkins, S. Gor, N. Cantu-Medellin, E. R. Weidert, et al. 2014. Fatty acid nitroalkenes ameliorate glucose intolerance and pulmonary hypertension in high-fat diet-induced obesity. *Cardiovasc. Res.* **101:** 352–363.

26. Zou, W. 2011. Separation of lipids by solid phase extraction (SPE). Accessed December 15, 2016, at http://www.nature.com/protocolexchange/protocols/2156.

27. Pietsch, A., and R. L. Lorenz. 1993. Rapid separation of the major phospholipid classes on a single aminopropyl cartridge. *Lipids.* **28:** 945–947.

28. Aveldaño, M. I., and L. A. Horrocks. 1983. Quantitative release of fatty acids from lipids by a simple hydrolysis procedure. *J. Lipid Res.* **24:** 1101–1105.

29. Rudolph, V., F. J. Schopfer, N. K. Khoo, T. K. Rudolph, M. P. Cole, S. R. Woodcock, G. Bonacci, A. L. Groeger, F. Golin-Bisello, C. S. Chen, et al. 2009. Nitro-fatty acid metabolome: saturation, desaturation, beta-oxidation, and protein adduction. *J. Biol. Chem.* **284:** 1461–1473.

30. Zinser, E., C. D. Sperka-Gottlieb, E. V. Fasch, S. D. Kohlwein, F. Paltauf, and G. Daum. 1991. Phospholipid synthesis and lipid composition of subcellular membranes in the unicellular eukaryote Saccharomyces cerevisiae. *J. Bacteriol.* **173:** 2026–2034.

31. Fernández-Murray, J. P., and C. R. McMaster. 2007. Phosphatidylcholine synthesis and its catabolism by yeast neuropathy target esterase 1. *Biochim. Biophys. Acta.* **1771:** 331–336.

32. Jain, S. S., S. Paglialunga, C. Vigna, A. Ludzki, E. A. Herbst, J. S. Lally, P. Schrauwen, J. Hoeks, A. R. Tupling, A. Bonen, et al. 2014. High-fat diet-induced mitochondrial biogenesis is regulated by mitochondrial-derived reactive oxygen species activation of CaMKII. *Diabetes.* **63:** 1907–1913.

33. Paglialunga, S., A. Ludzki, J. Root-McCaig, and G. P. Holloway. 2015. In adipose tissue, increased mitochondrial emission of reactive oxygen species is important for short-term high-fat diet-induced insulin resistance in mice. *Diabetologia.* **58:** 1071–1080.

34. Kawasaki, N., R. Asada, A. Saito, S. Kanemoto, and K. Imaizumi. 2012. Obesity-induced endoplasmic reticulum stress causes chronic inflammation in adipose tissue. *Sci. Rep.* **2:** 799.

35. O'Donnell, V. B., J. P. Eiserich, A. Bloodsworth, P. H. Chumley, M. Kirk, S. Barnes, V. M. Darley-Usmar, and B. A. Freeman. 1999. Nitration of unsaturated fatty acids by nitric oxide-derived reactive species. *Methods Enzymol.* **301:** 454–470.

36. Kansanen, E., H. K. Jyrkkanen, O. L. Volger, H. Leinonen, A. M. Kivela, S. K. Hakkinen, S. R. Woodcock, F. J. Schopfer, A. J. Horrevoets, S. Yla-Herttuala, et al. 2009. Nrf2-dependent and -independent responses to nitro-fatty acids in human endothelial cells:

37. Cui, T., F. J. Schopfer, J. Zhang, K. Chen, T. Ichikawa, P. R. Baker, C. Batthyany, B. K. Chacko, X. Feng, R. P. Patel, et al. 2006. Nitrated fatty acids: Endogenous anti-inflammatory signaling mediators. *J. Biol. Chem.* **281:** 35686–35698.

identification of heat shock response as the major pathway activated by nitro-oleic acid. *J. Biol. Chem.* **284:** 33233–33241.

38. Li, Y., J. Zhang, F. J. Schopfer, D. Martynowski, M. T. Garcia-Barrio, A. Kovach, K. Suino-Powell, P. R. Baker, B. A. Freeman, Y. E. Chen, et al. 2008. Molecular recognition of nitrated fatty acids by PPAR gamma. *Nat. Struct. Mol. Biol.* **15:** 865–867.

39. Rudolph, T. K., T. Ravekes, A. Klinke, K. Friedrichs, M. Mollenhauer, M. Pekarova, G. Ambrozova, H. Martiskova, J. J. Kaur, B. Matthes, et al. 2016. Nitrated fatty acids suppress angiotensin II-mediated fibrotic remodelling and atrial fibrillation. *Cardiovasc. Res.* **109:** 174–184.

40. Ambrozova, G., H. Martiskova, A. Koudelka, T. Ravekes, T. K. Rudolph, A. Klinke, V. Rudolph, B. A. Freeman, S. R. Woodcock, L. Kubala, et al. 2016. Nitro-oleic acid modulates classical and regulatory activation of macrophages and their involvement in pro-fibrotic responses. *Free Radic. Biol. Med.* **90:** 252–260.

41. Rudolph, T. K., V. Rudolph, M. M. Edreira, M. P. Cole, G. Bonacci, F. J. Schopfer, S. R. Woodcock, A. Franek, M. Pekarova, N. K. Khoo, et al. 2010. Nitro-fatty acids reduce atherosclerosis in apolipoprotein E-deficient mice. *Arterioscler. Thromb. Vasc. Biol.* **30:** 938–945.

42. Liu, H., Z. Jia, S. Soodvilai, G. Guan, M. H. Wang, Z. Dong, J. D. Symons, and T. Yang. 2008. Nitro-oleic acid protects the mouse kidney from ischemia and reperfusion injury. *Am. J. Physiol. Renal Physiol.* **295:** F942–F949. [Erratum. 2014. *Am. J. Physiol. Renal Physiol.* **306:** F1391.]

43. Cole, M. P., T. K. Rudolph, N. K. Khoo, U. N. Motanya, F. Golin-Bisello, J. W. Wertz, F. J. Schopfer, V. Rudolph, S. R. Woodcock, S. Bolisetty, et al. 2009. Nitro-fatty acid inhibition of neointima formation after endoluminal vessel injury. *Circ. Res.* **105:** 965–972.

44. Schopfer, F. J., M. P. Cole, A. L. Groeger, C. S. Chen, N. K. Khoo, S. R. Woodcock, F. Golin-Bisello, U. N. Motanya, Y. Li, J. Zhang, et al. 2010. Covalent peroxisome proliferator-activated receptor gamma adduction by nitro-fatty acids: selective ligand activity and anti-diabetic signaling actions. *J. Biol. Chem.* **285:** 12321–12333.

45. Schopfer, F. J., C. Cipollina, and B. A. Freeman. 2011. Formation and signaling actions of electrophilic lipids. *Chem. Rev.* **111:** 5997–6021.

46. Batthyany, C., F. J. Schopfer, P. R. Baker, R. Duran, L. M. Baker, Y. Huang, C. Cervenansky, B. P. Branchaud, and B. A. Freeman. 2006. Reversible post-translational modification of proteins by nitrated fatty acids in vivo. *J. Biol. Chem.* **281:** 20450–20463.

47. Vitturi, D. A., C. S. Chen, S. R. Woodcock, S. R. Salvatore, G. Bonacci, J. R. Koenitzer, N. A. Stewart, N. Wakabayashi, T. W. Kensler, B. A. Freeman, et al. 2013. Modulation of nitro-fatty acid signaling: prostaglandin reductase-1 is a nitroalkene reductase. *J. Biol. Chem.* **288:** 25626–25637.

48. Salvatore, S. R., D. A. Vitturi, M. Fazzari, D. K. Jorkasky, and F. J. Schopfer. 2017. Evaluation of 10-nitro oleic acid bio-elimination in rats and humans. *Sci. Rep.* **7:** 39900.

49. Alexander, R. L., D. J. Bates, M. W. Wright, S. B. King, and C. S. Morrow. 2006. Modulation of nitrated lipid signaling by multidrug resistance protein 1 (MRP1): glutathione conjugation and MRP1-mediated efflux inhibit nitrolinoleic acid-induced, PPARgamma-dependent transcription activation. *Biochemistry.* **45:** 7889–7896.

50. Baker, L. M., P. R. Baker, F. Golin-Bisello, F. J. Schopfer, M. Fink, S. R. Woodcock, B. P. Branchaud, R. Radi, and B. A. Freeman. 2007. Nitro-fatty acid reaction with glutathione and cysteine. Kinetic analysis of thiol alkylation by a Michael addition reaction. *J. Biol. Chem.* **282:** 31085–31093.

51. Bates, D. J., M. O. Lively, M. J. Gorczynski, S. B. King, A. J. Townsend, and C. S. Morrow. 2009. Noncatalytic interactions between glutathione S-transferases and nitroalkene fatty acids modulate nitroalkene-mediated activation of peroxisomal proliferator-activated receptor gamma. *Biochemistry.* **48:** 4159–4169.

52. McArthur, M. J., B. P. Atshaves, A. Frolov, W. D. Foxworth, A. B. Kier, and F. Schroeder. 1999. Cellular uptake and intracellular trafficking of long chain fatty acids. *J. Lipid Res.* **40:** 1371–1383.

53. Golej, D. L., B. Askari, F. Kramer, S. Barnhart, A. Vivekanandan-Giri, S. Pennathur, and K. E. Bornfeldt. 2011. Long-chain acyl-CoA synthetase 4 modulates prostaglandin E(2) release from human arterial smooth muscle cells. *J. Lipid Res.* **52:** 782–793.